The application of terrestrial laser scanner and SfM photogrammetry in measuring erosion and deposition processes in two opposite slopes in a humid badland area (Central Spanish Pyrenees)

Nadal Romero, E. (1), Revuelto, J. (2), Errea, P. (2), López Moreno, J.I. (2)

(1) Institute for Biodiversity and Ecosystem Dynamics. Earth Surface Science Research Group (IBED-ESS). University of Amsterdam, Amsterdam, Netherlands. M.E.NadalRomero@uva.nl

(2) Instituto Pirenaico de Ecología (CSIC). Procesos Geoambientales y Cambio Global, Zaragoza, Spain.

Abstract

Erosion and deposition processes in badland areas are usually estimated using traditional observations of topographic changes, measured by erosion pins or profile meters (invasive techniques). In recent times, remote-sensing techniques (non-invasive) have been routinely applied in geomorphology studies, especially in erosion studies. These techniques provide the opportunity to build high-resolution topographic models at centimeter accuracy. By comparing different 3D point clouds of the same area, obtained at different time intervals, the variations in the terrain and temporal dynamics can be analyzed. The aim of this study is to assess and compare the functioning of Terrestrial Laser Scanner (TLS, RIEGL LPM-321) and Structure-from-Motion photogrammetry (SfM) techniques (Camera FUJIFILM, Finepix x100 and Software PhotoScan by AgiSoft), to evaluate erosion and deposition processes in two opposite slopes in a humid badland area in the Central Spanish Pyrenees. Results showed that TLS data sets and SfM photogrammetry techniques provide new opportunities in geomorphological erosion studies. The data we recorded over one year demonstrated that north-facing slopes experienced more intense and faster changing geomorphological dynamics than south-facing slopes as well as the highest erosion rates. Different seasonal processes were observed, with the highest topographic differences observed during winter periods and the high intensity rainfalls in summer. While TLS provided the highest accuracy models, SfM photogrammetry was still a faster methodology in the field and precise at short distances. Both techniques present advantages and disadvantages, and do not require direct

contact with the soil and thus prevent the usual surface disturbance of traditional and invasive methods.

Keywords: badlands, remote sensing techniques, Terrestrial Laser Scanner, Structure-from-Motion photogrammetry, geomorphological processes

1. Introduction

1.1. Humid badlands: strong geomorphological dynamics

Previous studies defined badlands as areas with scarce or no vegetation, where human activities, especially agriculture, are not possible (e.g. Alexander, 1982; Bryan and Yair, 1982; Fairbridge, 1968; Howard, 1994). Although badlands are considered characteristics of arid and semiarid environments, they are also found in humid and subhumid areas (Gallart et al., 2013). Badlands are a landscape with a very high frequency and magnitude of geomorphological processes, resulting in rapid landscape evolution, which makes them "ideal field laboratories". Sheet wash erosion, gullies and rills, landslides, and mudflows are often observed in badland areas; the constantly changing landscape makes it very difficult to analyze geomorphological dynamics and measure erosion.

In general badland areas show high erosion rates. The recorded values depend on the applied methodologies (Sirvent et al., 1997), on the spatial scale of measurement (Nadal-Romero et al., 2011, 2014) and also on the temporal scale, as erosion rates show high inter-annual variability (García-Ruiz et al., 2015). A recent comprehensive review by Nadal-Romero et al. (2011, 2014) of the scale-dependency of sediment yields from badland areas in Mediterranean environments showed extensive variability in erosion rates and sediment yields. In the Tabernas Badlands, Cantón et al. (2001) measured very low erosion rates (0.08–0.35 mm yr^{-1}) due to the low frequency of rainfall. Lam (1977) obtained 17.36 mm yr^{-1} in the Hong Kong badlands. Higher values were registered in subhumid badland areas of southern Tuscany (15–20 mm yr^{-1}) (Cicacci et al., 2008) and the Prealps catchments in France, with erosion rates of over 30 mm yr^{-1} (Chodzko et al., 1991). Recently, Vericat et al. (2014), using a non-invasive technology, a Terrestrial Laser Scanner (TLS), measured an annual soil loss of around 60 mm yr^{-1} in the Eastern Pyrenees (Spain).

1.2. Review: Methodologies for analyzing geomorphological processes and erosion rates in badlands

The geomorphology of badlands has been extensively studied for the last 30 years, and there is a substantial body of literature on the subject. In this context, numerous methods have been used to understand geomorphological dynamics (erosion and deposition processes) and quantify erosion rates. The following presents an overview of the main methodologies for investigating erosion rates and sediment yields in badlands.

A total of 171 papers (starting from 1956) were identified using the Scopus and the ISI Web of Knowledge databases (search terms: "Badlands and erosion rates" and "Badlands and Sediment Yield"). The obtained information enables the classification of the studies according to the different methods (Figure 1).

The analysis showed that there is no standard protocol for measuring erosion and sediment yield in badland areas, with a variety of methods (at different temporal and spatial scales) being used, both conventional and new remote sensing techniques. The most commonly reported method is a gauging station (e.g. Nadal-Romero et al., 2008), seen by different authors as the best approach for measuring sediment transport (Walling, 1991). Remote sensing technologies (e.g. Martínez-Casasnovas and Ramos, 2009), rainfall simulations (e.g. Martínez-Murillo et al., 2013) and erosion models (e.g. Mathys et al., 2003) were recorded in about 20 studies. Topographic surveys (e.g. Sirvent et al., 1997), runoff plots (e.g. Gallart et al., 2013) and erosion pins (e.g.. Vergari et al., 2013) were used a bit less often (approximately 15 studies each). On the other hand, dendrogeomorphological techniques (e.g. Ballesteros-Canovas et al., 2013), TLS data acquisition (e.g. Sáez et al., 2011; Vericat et al., 2014), radioisotopic measurements (e.g. Sadiki et al., 2007) and bathymetric surveys (e.g. Grauso et al., 2008) have been sporadically applied in badland studies (Figure 1).

The methods were classified as invasive tools (mostly traditional methods, e.g. gauging station, rainfall simulations, topographic surveys, runoff plots, erosion pins) and non-invasive tools (mostly new technologies, e.g. remote sensing, TLS, SfM photogrammetry, aerial pictures). The annual evolution of the different methods is represented in Figure 2 (data from 1980, n = 164). Figure 2 indicates that (i) during the last 30 years, studies on soil erosion in badlands have increased (see also Gallart et al., 2013); (ii) the few studies during the 1980s all used traditional invasive tools; and (iii) from 1996, non-invasive methods are starting to be used in erosion studies in badland areas, with the sharpest increase in 2007.

1.3. New remote-sensing techniques: Terrestrial Laser Scanner and SfM photogrammetry

Field methods for geomorphological processes analysis and soil erosion quantification have evolved from traditional methods (most of them invasive) to those that do not disturb the soil (non-invasive). In the last decades, techniques to rapidly acquire high-density topographic data have proliferated; however, the tools to adequately analyze change within these complex data sets have only now become accessible (Barnhart and Crosby, 2013).

Terrestrial Laser Scanners (TLS) are a non-intrusive, high precision tool, designed to retrieve information on the topographic characteristics of any surface. TLS use LiDAR technology (Light Detecting and Ranging), to accurately measure the distance from the device to the desired surface. By measuring the distance at thousands of points, 3D point clouds of a very high spatial resolution are obtained. This information makes it possible to generate Digital Elevation Models (DEMs) that accurately reproduce the topographic surfaces. TLS serves as a monitoring tool to observe changes in surface morphology, and the data collected with TLS can be used for both calculations of volumetric changes as well as documentation of surface conditions (development of rills, roughness etc.). The acquisition time is relatively short, and the precision is sufficient for detailed erosion studies in very active areas. The high-resolution topographical data already obtained with TLS in badland areas (e.g.. Lucía et al., 2011; López-Saez et al., 2011; Vericat et al., 2014) encourage its application in other study sites.

Digital photogrammetry has generated an improvement in topographic methods, due to a better accessibility to a wider variety of users, its low cost, and also due to the increased automation of the photogrammetric routines (Fonstad et al., 2013). Recently, Structure for Motion (SfM) techniques, developed by the computer vision community, were adapted to generate high resolution and quality DTMs. Classical (stereoscopic) photogrammetry is based on 3D reconstruction models by superimposing two images of the same area from different perspectives. SfM is based on the reconstruction of the 3-dimensional geometry from the matching of multiples images generated from different points of view. Pictures can be taken at different scales, and the position, orientation and distortion can be unkown. SfM differs from stereoscopic photogrammetry, because it uses image matching algorithms to recover randomly acquired images and to detect points in common elements.

The biggest difference between both methods is the need to use GCPs for the 3D model resolution. In classical photogrammetry, the collinearity is solved after the introduction of the GCPs; in SfM, collinearity is solved from the common elements of the images. So, if there are errors in the measurements of the GCPs, they are propagated to the final result (Fonstad et

al., 2013). Through SfM, the final quality of the point cloud is based on a high number of common points (> 1000) that have been automatically generated.

The information from either aerial or terrestrial photographs is processed using one of a number of available software solutions, creating 3D point clouds from several images of one area. Today, this tool offers new possibilities and innovative procedures, like creating DEMs in automatic mode to reconstruct surfaces (Bitelli et al., 2004). During the past 20 years, intensive research was published on the automation of the information extraction from digital images (e.g. the continuous development of processing algorithms) (Baltsavias, 1999). Several scientific fields, like geoarcheology and architecture, have already accepted photogrammetry as a useful tool (e.g. Cardenal Escarcena et al., 2011; Verhoeven et al., 2012; Martínez et al., 2015; Nadel et al., 2015), and its advantages for geomorphological research have been long recognized (Castillo et al., 2012). In the last five years various studies have taken advantage of the possibilities offered by geomorphology to generate terrain models using SfM photogrammetry (Gómez-Gutierrez et al., 2014, Kaiser et al., 2014, Michetti et al., 2015, Westoby et al., 2012).

The main objective of this research is to assess and compare Terrestrial Laser Scanner (TLS) and Structure-from-Motion photogrammetry methods for the evaluation of geomorphological processes (erosion and deposition) and topographic changes in two opposite active slopes (north- and south-facing) in a humid badland area in the Central Spanish Pyrenees. Annual topographic changes will be evaluated and geomorphological processes will be spatially analyzed.

2. Materials and methods

2.1. Study area: The Araguás catchment

The Araguás catchment (0.45 km^2) is a north-south orientated tributary of the Lubierre River, located in the Central Spanish Pyrenees. The altitude ranges from 780 to 1,105 m, and it has a substantially large badland area, spreading over 25% of the catchment (Figure 3).

The climate of the area is sub-Mediterranean with Atlantic and Continental influences (Creus, 1983). The average annual rainfall is about 800 mm, varying from 500 to 1,000 mm annually, and the average temperature is 10 ºC.

Badlands occur on the Eocene marl of the Inner Pyrenean Depression (marls with interbedded decimeter-scale sandy layers). Nadal-Romero and Regüés (2010) demonstrated that the main causes of regolith development and weathering processes are the alternating

freeze-thaw and wetting-drying cycles (being maximum in winter and summer).

The Araguás catchment has been monitored since 2004 to study the hydrological and sedimentological dynamic in the badland area, using a gauging station at the outlet of the catchment. Previous studies showed that the dynamics of weathering and erosion processes are the principal factors controlling geomorphological development, showing extreme hydrological and sedimentological responses (Nadal-Romero and Regüés, 2010). The badlands are very active: intense sheet wash erosion, gullying and rilling, with heavy mudflows during the most intense rainstorms, produce substantial annual sediment yields (Nadal-Romero et al., 2008).

Two slopes with opposite aspect (facing north and south) were selected to apply the TLS and photogrammetric surveys (Figure 3). These slopes were chosen based on two criteria: (1) according to the different geomorphological processes that can be observed on the dry slope (south-facing) and on the more humid one (north-facing), and (2) according to the differences in the surveyed areas and on the working distances for data acquisition with both methods (TLS and SfM). The analyzed extension of the north and south slopes are 3,200 m^2 and 560 m^2, respectively. The average working distance for the TLS in the north-facing slope is 102 m, while for the south-facing slope is 25 m. The pictures for the SfM photogrammetry software were taken from an average distance of 100–150 m for the north-facing slope, and 40–60 m for the south-facing slope.

2.2. Terrestrial Laser Scanner

The device used in the present study is a long-range TLS (RIEGL LPM-321) (see Revuelto et al., 2014 for checking the technical characteristics of the TLS and the procedure used for scanning and for the post-processing information).

Indirect registration (target-based registration) was used to merge the information from the different scan station and for transforming the local coordinates of the obtained point clouds into a global coordinate system. The point cloud transformation makes it possible to compare scans made on different survey days. The indirect registration considers fixed reflective targets placed at reference points (metallic stakes), which are placed at the same positions at the study site. We installed 9 targets on the north-facing slope and 9 targets on the south-facing slope (the high number of targets increases the robustness of the experimental setup, see Revuelto et al., 2014), each was a cylindrical reflector 0.10 m in

198 diameter placed at a height of 0.10 m. TLS automatically obtains 3D point clouds, but with a
199 main limitation, we have only work from a single position due to time restrictions.
200 Once the formal steps were completed (e.g. atmospheric correction, scan of targets,
201 selection and delimitation of the area of interest), we started with the scan of the selected
202 slopes.
203 In this study, on the north-facing slope the average resolution in point cloud acquisition
204 was 625 points/m^2 (0.04 m linear distance between points), and the angular scanning
205 resolution was 0.027º. On the south-facing slope the resolution was, 1,890 points/m^2
206 (0.023 m) and the angular scanning resolution was 0.054º. For the areas closer to the TLS, the
207 point resolution increased while at longer distances decreased. This is one of the main
208 limitations of the technology: it does not enable a consistent distribution of the acquired
209 information.
210 Finally, when the scan was completed, photographs were taken using a digital camera
211 coupled to the scanner, to capture useful RGB (Red, Green, Blue) information for each point.
212
213 *2.3. Structure-from-Motion photogrammetry*
214 Structure-from-Motion photogrammetry allows the creation of 3D models from multiple
215 overlapping images taken at distinct triangulation angles. In this case, we used the FUJIFILM
216 Finepix x 100 camera, with a focal length of 23 mm (equivalent to a fixed lens of 35 mm),
217 with a resolution of 12 MP (4288 x 2848 pixels).. In each survey, 17 pictures of the north-
218 facing slope were taken at an approximate distance of 100-150 m; 15 pictures of the south-
219 facing slope were taken, at an approximate distance 40–60 m.. The pictures were taken by
220 hand following a set-walking itinerary. The images were analyzed with Agisoft Photoscan
221 Professional Edition® software, generating a 3D point cloud of the study area. Differences in
222 lighting can cause problems during data processing, and Agisoft software is a helpful tool to
223 overcome this risk, as it estimates the potential error and deletes questionable pictures. The
224 spatial resolution of the generated point clouds depends on the quality of the model processed
225 with the images obtained with the camera. In this study, we used higher resolution modes,
226 which provided a spatial resolution of 970 points/m^2 for the north-facing slope, and 2800
227 points/m^2 for the south-facing slope. High resolution of original images would offer better
228 texture and higher resolution to find keypoints in the photoset. Similarly, decreasing the
229 distance between the camera and the feature of interest is related to increasing the spatial
230 resolution of the photograph and would enhance the spatial density and resolution of the final
231 point cloud (Westoby et al., 2012).

232

233 *2.4.Data processing*

234 In order to georeference both data sets (SfM photogrammetry and TLS point clouds) into the
235 same coordinate system, we applied indirect registration (target-based) using the reference
236 point coordinates of the targets (coordinates acquired with the TLS). Based on the target
237 coordinates, a transformation matrix to a common coordinate system (which is named project
238 coordinate system)using Riprofile 1.6.2 software is generated for the TLS point cloud. The
239 standard deviation was lower than 0.015 m in all the TLS scans, which is in accordance to
240 errors reported in other studies (Revuelto et al., 2014; Prokop, 2008). Similarly, the point
241 cloud obtained from SfM photogrammetry is transformed onto the same coordinate system by
242 a transformation matrix calculated in Agisoft Photoscan using the TLS-recorded target
243 coordinates with standard deviation below 0.025 m. The transformation of the coordinates
244 into a common coordinate system was carried out for the comparison of the information
245 obtained with the two methods.

246 In both cases, the post-processing (comparing point clouds to determine the topographic
247 differences between dates) was accomplished using CloudCompare software (Girardeau-
248 Monaut et al., 2005), which generates maps of distances between clouds of points
249 corresponding to different survey days.

250 Measurements were performed at similar intervals between July 2013 and July 2014; in
251 total four topographic surveys of each study zone were conducted on the following dates: 24
252 July 2013, 12 November 2013, 26 March 2014 and 24 July 2014.

253 Rainfall data was recorded in the Araguás catchment (see Nadal-Romero and Regüés,
254 2010) and the volume and characteristics of rainfall during the study periods was also
255 analyzed.

256

257 **3. Results**

258

259 Data analyses are conducted on different temporal scales – (i) survey/monitoring intervals,
260 and (ii) at annual scale in both slopes (north- and south-facing slopes) – using both TLS and
261 SfM photogrammetry. Monitoring intervals and rainfall data are presented in Table 1 and
262 Figure 4. The length of the monitoring intervals ranged from 112 to 134 days. Maximum
263 daily rainfall was from 24.6 to 77.2 mm, and the maximum 5-min rainfall intensity ranged
264 from 14.4 to 148.8 mm h^{-1}.

The results are structured in 3 sections. First, the results obtained on the north-facing slopes are analyzed (Section 3.1), and then the results obtained on the south-facing slope are examined (Section 3.2). In both sections, spatial and temporal variability of topographic changes are described. Finally (Section 3.3), a comparison between both data analysis and methodologies is carried out.

3.1. North-facing slopes

Observed topographic changes over different monitoring survey intervals on the north-facing slope are presented in Figures 5 and 6 (TLS and SfM photogrammetry data respectively). Erosion and deposition values are summarized in Table 2. Negative values reflect erosion processes. On the other hand, positive values may reflect deposition processes; however, swelling processes can also influence these values (Vericat et al., 2014).

On north-facing slopes, period 2 (longest period, winter period) showed the strongest and most variable topographic changes (Figures 5 and 6): -0.046 m and -0.051 m with TLS and SfM photogrammetry respectively. Most sections of the slope showed signs of rills development.

However, the biggest absolute differences were observed during period 1 (summer). It was the rainiest period (334.8 mm) due to convective storms with high rainfall intensities (148.8 mm h^{-1}, see Table 1). During this period the maximum negative difference (-0.610 m and -0.43 m with TLS and SfM photogrammetry respectively) was registered due to small movements in the upper part of the slope. A small zone of regolith deposits was also evident just downhill of this movement (Period 1, Figures 5 and 6). Period 3 (spring) showed the lowest values, which is consistent with the low rainfall (198 mm).

3.2. South-facing slopes

On south-facing slopes, period 2 showed the biggest and most variable topographic changes (Figures 7 and 8, and Table 3): -0.037 m and -0.001 m (note the high standard deviation compared to the average difference in Table 1) with TLS and SfM photogrammetry respectively. An important movement was recorded on the lower part of the slope, showing high positive and negative values (both erosion and deposition).

The changes in periods 1 and 3 were smaller, although important rill development was observed in both periods. Small movements and deposition processes at footslopes were recorded (see Figures 7 and 8).

298 On the south-facing slope the biggest absolute differences were also observed during
299 period 2, due to the important movement recorded at the lower part of the slope. The
300 maximum negative difference was around -0.42 m, while the maximum positive difference
301 was around 0.50 m.
302
303 *3.3. Joint analysis*
304 The magnitude of the annual erosion rates was higher on the north-facing slope than on the
305 south-facing slope, -0.077 m and -0.032 m respectively, recorded using TLS point clouds (see
306 Table 2 and 3). SfM photogrammetry yielded more moderate differences: -0.017 m and -
307 0.002 m on the north-facing and south-facing slope respectively. Furthermore, on the south-
308 facing slope the annual maximum negative and positive values are very similar (0.416 m and
309 -0.453 m with TLS, and 0.48 m and -0.42 m with SfM photogrammetry); however, important
310 differences were observed between the negative and positive absolute maximum values on
311 north-facing slopes (0.250 m and -0.590 m with TLS, and 0.34 m and -0.46 m with SfM
312 photogrammetry).
313 In both cases, the variability of topographic changes was very high, as indicated by the
314 high standard deviations (which was even higher at the south-facing slope).
315 If differences between both methods are analyzed, we have to highlight that in south-
316 facing slopes (short distance and small area) the values using both methodologies are really
317 similar; however, on the north-facing slope (long distance and large area) the measurement
318 differences between the two methodologies are remarkable.

319 Figures 9 and 10 showed a direct comparison of DEMs between techniques considering
320 LiDAR (TLS) as the reference. Differences have been calculated for the first and last
321 acquisition dates (23/07/13 and 23/07/14). Big differences occurred in small areas, where
322 small vegetation patches were present (almost all vegetation was eliminated from the point
323 clouds, but some influence can be appreciated in the exterior limits of the selected slopes).
324 Small differences were observed in “deep” concavities (yellow colours in the comparison
325 figures), because in these areas the SfM was not able to accurately reproduce a precise
326 topography. Other errors were usually located in ridges, and the areas behind them, from the
327 TLS perspective, showing one of the main TLS limitations: with only one point of view,
328 some areas are hidden. Average differences (Table 4) were higher in north-facing slopes (also
329 the highest standard deviation were recorded in this slope) in both surveys because the
330 increase on distance of data acquisition and the presence of shadows..

4. Discussion

4.1. Geomorphological dynamics

Both techniques can produce high-resolution topographic models with centimeter accuracy. By comparing different point clouds of the same area, obtained at different time periods, we analyzed variations in the topographic characteristics of the terrain and the temporal geomorphological dynamics.

First, it must be highlighted that the variability of the recorded topographic changes was very high, as reflected by the high standard deviation (see Table 2 and 3). The detailed analysis of the point clouds showed the geomorphological dynamics of these severely eroded areas. The results indicated that the geomorphological dynamics on north-facing slopes were more intense than on south-facing slopes, except punctual high variations on the south-face. Various studies have highlighted terrain aspect as an important factor in the geomorphological development of badlands (e.g. Calvo-Cases and Harvey, 1996; Descroix and Olivry, 2002; Pulice et al., 2013).

The values presented in Table 2 and 3 also showed that highest topographic changes were recorded during winter periods. Also other studies highlighted that the development and weathering dynamics of regolith in north-facing slopes are more active in winter, due to the freeze–thaw weathering processes, while south-facing slopes are dominated by the development of crusts associated with wetting–drying processes (Nadal-Romero et al., 2007; Nadal-Romero and Regüés, 2010). It has to be noted that shrink–swelling and freeze–thaw processes may cause dilation of surface material, which results in a net surface elevation; however, this study did not take these small variations into account.

North-facing slopes experienced small mud or debris flows, although also south-facing slopes had these flows due to the high slope gradient (Figures 9 and 10), showing the importance of climate and topographic factors in badlands development. These types of movements have also been recorded in humid badlands in southeast France using a small portable camera in the Draix catchment (Miniature Debris Flows – MDF) (Yamakoshi et al., 2009). Nadal-Romero et al. (2007), based on field evidence and laboratory work, suggested that in these badland morphologies shallow landslides and small mudflows commonly occur during prolonged rainfall events. These erosion processes produced the development of fans at the base of slopes and near the main channels, processes also observed in different badland morphologies (Balasch, 1998; Regüés and Gallart, 2004; Desir and Marín, 2007). It is also

remarkable that during summer, convective storms of high intensity and short duration overcome infiltration capacity and generate intense concentrated runoff. Rills and gully development usually appear during these events and are significant in sediment production (Nadal-Romero and Regüés, 2010). Both TLS and SfM photogrammetry captured these processes, which confirms that both are good techniques for studying geomorphological processes in badland areas.

TLS results on the north-facing slope indicated a negative difference of 77 mm yr^{-1}, while on the south-facing slope the negative values are lower, 32 mm yr^{-1}. More moderate differences are recorded using SfM photogrammetry point clouds with annual values of 17 mm yr^{-1} and 2 mm yr^{-1}, on the north-facing and south-facing slopes respectively. Nevertheless these values should be contextualized with the observed standard deviation of 38 mm for north-facing and 56 mm for south-facing slopes. Nadal-Romero et al. (2008) estimated erosion rates (represented as a lowering of the soil surface) determined from the suspended sediment loss measured at the outlet of the catchment (converted to centimeters) and taking into account the specific weight of the marl (2.75 g/cm^{-3}). During the study period (November 2005 to January 2007), March and September 2006 were particularly active in terms of sediment transport, with a recorded drop in soil surface of 13 and 8 mm, respectively. The estimate of annual erosion rates for the entire catchment was 27.5 mm yr^{-1}. High erosion rates, similar to the ones obtained in this study, were recorded in different badland areas. Using similar methodology, Vericat et al. (2014) measured an annual change of around minus 60 mm yr^{-1} in the Eastern Pyrenees (Spain). Lower values were registered in subhumid badland areas of southern Tuscany (15–20 mm yr^{-1}) (Cicacci et al., 2008) and the Prealps catchments in France (over 30 mm yr^{-1}) (Chodzko et al., 1991) using invasive traditional methodologies.

4.2. New non-invasive tools

This study demonstrates that both methodologies adequately facilitate subsequent analysis – both in a quantitative (metric) and qualitative (interpretive) way. Both offer a good opportunity to safely measure landform without soil disturbance, with high spatial resolution and in a relative short time period. Table 5 presents the advantages and disadvantages of both methods.

Both methods allow fast and automatic image processing. Nevertheless, SfM photogrammetry reduces the data collection effort in the field, although post-processing is still labor-intensive. TLS is an expensive (and quite heavy) tool, while SfM photogrammetry

is relatively cheap and easy to use. Castillo et al. (2012) calculated the cost of TLS at 10 times the cost of 3D photogrammetry.

The comparison between both methods (Figures 9 and 10 and Table 4) showed that results were similar in both cases, although significant differences can be observed in small points, especially in the presence of shadows and vegetation.

Our study demonstrated that SfM delivers good accuracy and is really useful for field application in geomorphological and soil erosion studies, for observing changes in the centimeter scale (depending on the working distance). In our case, the quality of the images should be improved in order to obtain better accuracy, paying special attention to illumination changes during the acquisition of the images, which have been observed as an important error-causing interference. The number of pictures could be a problem to be solved together with the computer memory (a large memory is needed to process a large number of high quality pictures). Nevertheless, if the image acquisitions locations are well established and the image overlapping is done well, the number of needed images is not very high (5–10 pictures). Micheletti et al. (2015) carried out an analyses in similar areas and at the same scale, and they obtained good and valid models with 13 pictures.

TLS shows better performance in differentiating small displacement of terrain (resolution of surface models) (e.g. rills development). However, due to time restrictions we have worked with one single scan position causing the shadowing effect of terrain (the so-called sight shadowing), which does not allow to retrieve data from different areas of the site originating missing information. This missing information due to terrain curvature observed in some areas with the TLS (north-slope), is avoided with SfM photogrammetry because different points of view of the study area were easily acquired (see differences in Figures 9 and 10). Nevertheless, in the presented analyses, and annual erosion rates these shadow areas have been removed in SfM photogrammetry to consider exactly the same area with both methods.

SfM photogrammetry performs better for the spatial distribution of the point cloud, for areas closer to the TLS the point resolution is increased, while for longer distances it is decreased, which is one of the main limitations of this technology. However, TLS does provide higher resolution of surface models. Indeed, the high number of points obtained for low distances to the TLS in comparison to these obtained for large distances is one limitation for these devices. This has encouraged minimizing scan distances when possible (Heritage and Hetherington, 2007). On the contrary, the SfM technique does not show this high

dependence on distance due to the multiple points of view of the surveyed area (Smith and Vericat, 2015). This is one of the main advantages when compared to TLS.

TLS and SfM photogrammetry data sets supported quantifiable data that previously had to be gathered through very labor- and time-intensive field measurement. Castillo et al. (2012) compared the accuracy, time and cost of the conventional and the new techniques. They observed that SfM photogrammetry is the method that produces the best approximation to the TLS. They also suggested that traditional methods (2D methods) can produce significant volume errors. Marzolff and Poesen (2009) suggested that compared to remote sensing imagery field methods have the disadvantages of time consuming measurements, thus usually covering rather small areas with a limited sampled density. Perroy et al. (2010) concluded that old methods (traditional and invasive) are time consuming, tedious, labor intensive and sometimes more expensive.

4.3. Future research

Further research needs to focus on analyzing geomorphological processes (erosion and deposition) and their controlling topographic (slope, aspect, roughness) and meteorological factors (rainfall and temperature) over a number of event–scale monitoring periods. During the new surveys a higher number of pictures will be taken, and TLS surveys will be taken from two single points. With this information we will check some of the observed limitations of both methodologies. The next stages of the project will focus also on the analysis and comparison of TLS and SfM photogrammetry data with data obtained with a new turbidimeter installed in the catchment at the beginning of 2015.

5. Conclusion

The study applied and compared the performance of the Terrestrial Laser Scanner and the photogrammetric technique in investigating the geomorphological dynamics and topographic changes on two active slopes in humid badland areas. TLS and SfM photogrammetry (non-intrusive methods) show high precision and obtain high-resolution topographic information. We used the combination of TLS and SfM photogrammetry to maximize their advantages while minimizing the disadvantages of each technique.

The results show that TLS and SfM photogrammetry data sets provide opportunities in the study of topographic change of very erosion-prone landscapes (e.g. badlands) where the use of conventional, invasive topographic technologies is limited. SfM photogrammetry is a powerful and low cost tool for evaluating the rate and spatial-temporal development of

465 denudation processes at short-distance and small areas. Small problems should be solved
466 using a camera with higher resolution, or a higher number of pictures. In that way, we could
467 consider that SfM photogrammetry would be a good opportunity in geomorphological studies
468 when carried out taking pictures at short distances.
469 The data recorded in the course of a year at different seasonal intervals demonstrated that
470 north-facing slopes experienced more intense and faster geomorphological dynamics than
471 south-facing slopes. Different seasonal processes were observed: the biggest topographic
472 differences coincided with the winter periods and the high intensity rainfall incidents in
473 summer.
474

475 **Acknowledgment**

476 Support for this research was provided by the project HIDROCAES (CGL2011-27574-C02-
477 01), INDICA (CGL2011-27753-C02-01) funded by the Spanish Ministry of Economy and
478 Competition. E. Nadal-Romero was the recipient of a Marie Curie IEF grant (Seventh EU
479 Framework Programme project "MED-AFFOREST" PIEF-GA-2013-624974). J. Revuelto
480 was the recipient of a FPU grant (Spanish Ministry).
481

482 **References**

483 Alexander, R.W.: Difference between 'calanchi' and 'biancane' badlands in Italy, in:
484 Badland Geomorphology and Piping, Bryan, R., Yair, A. (Eds.), Geobooks, Norwich, 71-
485 88, 1982.
486 Balasch, J.C.: Resposta hidrològica i sedimentària d'una petita conca de muntanya
487 analitzades at diferent escala temporal. PhD thesis, Universitat de Barcelona, 376 pp,
488 1998.
489 Ballesteros-Cánovas, J. A., Bodoque, J. M., Lucía, A., Martín-Duque, J. F., Díez-Herrero, A.,
490 Ruiz-Villanueva, V., Rubiales, J. M., and Genova, M.: Dendrogeomorphology in
491 badlands: Methods, case studies and prospects, Catena, 106, 113-122, 2013.
492 Baltsavias, E. P.: A comparison between photogrammetry and laser scanning, ISPRS-J.
493 Photogramm. Remote Sens., 54, 83-94, 1999.
494 Barnhart, T. B. and Crosby, B. T.: Comparing two methods of surface change detection on an
495 evolving thermo karst using high-temporal-frequency Terrestrial Laser Scanning, Selawik
496 River, Alaska, Remote Sens., 5, 2813-2837, 2013.

497 Bitelli, G., Dubbini, M., and Zanutta, A.: Terrestrial Laser Scanning and Digital
498 Photogrammetry techniques to monitor landslide bodies, in: XXth ISPRS Congress:
499 Proceedings of Commission V, Istanbul, Turkey, 246-251, 2004.
500 Bryan, R. and Yair, A.: Perspectives on studies of badland geomorphology, in: Badland
501 Geomorphology and Piping, Bryan, R. and Yair, A. (Eds.), Geobooks, Norwich, 1-12,
502 1982.
503 Calvo-Cases, A. and Harvey, A.M.: Morphology and development of selected badlands in
504 southeast Spain: Implications of climatic change, Earth Surf. Process. Landf. 21, 725-735,
505 1996.
506 Cantón, Y., Domingo, F., Solé-Benet, A., and Puigdefábregas, F.: Hydrological and erosion
507 response of a badlands system in semiarid SE Spain, J. Hydrol., 252, 65-84, 2001.
508 Cardenal Escarnena, J., Mata de Castro, E., Pérez García, J.L., Mozas Calvache, A.,
509 Fernández del Castillo, T., Delgado García, J., Ureña Cámara, M., Castillo, J. C.,:
510 Integration of photogrammetric and terrestrial laser scanning techniques for heritage
511 documentation, Virtual Archaeology Review, 2, 53-57.
512 Castillo, C., James, M.R., Redel-Macías, M.D., Pérez, R., and Gómez, J.A.: The SF3M
513 approach to 3-D photo-reconstruction for non-expert users: application to a gully network,
514 SOIL Discuss, 2, 371-399, 2015.
515 Castillo, C., Pérez, R., James, M.R., Quinton, J.N., Taguas, E.V., and Gómez, J.A.:
516 Comparing the Accuracy of Several Field Methods for Measuring Gully Erosion, Soil
517 Science Society of American Journal, 76 (4), 1319-1332, 2012.
518 Chodzko, J., Lecompte, M., Lhénaff, R., and Marre, A.: Vitesse de l'érosion dans les roubines
519 des Baronnies (Drôme), Physio-Géo, 22-23, 21-28, 1991.
520 Ciccacci, S., Galiano, M., Roma, M. A., and Salvatore, M.C.: Morphological analysis and
521 erosion rate evaluation in badlands of Radicofani area (southern Tuscany - Italy), Catena,
522 74 (2), 87-97, 2008.
523 CloudCompare software. http://www.danielgm.net/cc/
524 Creus, J.: El clima del Alto Aragón Occidental. Monografías del Instituto de Estudios
525 Pirenaicos 109. Consejo Superior de Investigaciones Científicas, Jaca, 1983.
526 Descroix, L. and Olivry, J.C.: Spatial and temporal factors of erosion by water of black marls
527 in the badlands of the French Southern Alps, Hydrol. Sci. J. 47 (2), 227-242, 2002.
528 Desir, G., and Marín, C.: Factors controlling the erosion rates in a semi-arid zone (Bardenas
529 Reales, NE Spain), Catena, 71, 31–40, 2007.

530 Fairbridge, R.W.: Encyclopedia of geomorphology, Stroudsburg, PA, Dowden, Hutchinson
531 and Ross, 1968.
532 Fonstad, M.A., Dietrich, J., Courville, B.C., Jensen, J., and Carbonneau, E.: Topographic
533 structure from motion: a new development in photogrammetric measurement, Earth
534 Surface Processes and Landforms, 38, 421-430, 2013.
535 Gallart, F., Marignani, M., Pérez-Gallego, N., Santi, E., and Maccherini, S.: Thirty years of
536 studies on badlands, from physical to vegetational approaches. A succinct review, Catena,
537 106, 4-11.
538 Gallart, F., Pérez-Gallego, N., Latron, J., Catari, G., Martínez-Carreras, N., and Nord, G.:
539 Short- and long-term studies of sediment dynamics in a small humid mountain
540 Mediterranean basin with badlands, Geomorphology, 196, 242-251, 2013.
541 García-Ruiz, J. M., Beguería, S., Nadal-Romero, E., González-Hidalgo, J. C., Lana-Renault,
542 N., and Sanjuán, Y.: A meta-analysis of soil erosion rates across the world,
543 Geomorphology, 239, 160-173,2015.
544 Girardeau-Montaut, D., Roux, R.M., and Thibault, G.: Change detection on points cloud data
545 acquired with a ground laser scanner, in: Workshop Laser Scanning 2005, ISPRS,
546 Enschede, the Netherlands, pp. 6, 2005.
547 Gómez-Gutiérrez, A., Schnabel, S., Berenguer-Sempere, F., Lavado-Contador, F., and Rubio-
548 Delgado, J.: Using 3D photo-reconstruction methods to estimate gully headcut erosion,
549 Catena, 120, 91–101, 2014.

550 Grauso, S., Pagano, A., Fattoruso, G., De Bonis, P., Onori, F., Regina P., and Tebano, C.:
551 Relations between climatic-geomorphological parameters and sediment yield in a
552 Mediterranean semi-arid area (Sicily, southern Italy), Environ. Geol., 54 (2), 219-234,
553 2008.
554 Heritage, G., and Hetherington, D.: Towards a protocol for laser scanning in fluvial
555 geomorphology, Earth Surface Processes and Landforms 32, 66–74, 2007.
556 Howard, A.D.: Badlands, in: Geomorphology of desert environments, Abrahams, A.D. and
557 Parsons, A.J., eds., Chapman and Hall, London, 213-242, 1994.
558 James, M.R. and Robson, S.: Straightforward reconstruction of 3D surfaces and topography
559 with a camera: Accuracy and geoscience application, J. Geophys. Res., 117, F03017,
560 doi:10.1029/2011JF002289, 2012.
561 Kaiser, A., Neugirg, F., Rock, G., Mueller, C., Haas, F., Ries, J., and Schmidt, J.: Small-
562 Scale Surface Reconstruction and Volume Calculation of Soil Erosion in Complex Mo-

563 roccan Gully Morphology Using Structure from Motion, Remote Sens., 6, 7050–7080,
564 2014.

565 Lam, K.: Patterns and rates of slope wash on the badlands of Hong Kong. Earth Surf.
566 Process. Landf., 2, 319-332, 1977.
567 López-Saez, J., Corona, C., Stoffel, M., Rovéra, G., Astrade, L., and Berger, F.: Mapping of
568 erosion rates in marly badlands based on a coupling of anatomical changes in exposed
569 roots with slope maps derived from LiDAR data, Earth Surf. Process. Landf., 36, 1162-
570 1171, 2011.
571 Lucía, A., Martín-Duque, J. F., Benjamin Laronne, J., and Sanz-Santos, M.A.: Geomorphic
572 dynamics of gullies developed in Sandy slopes of Central Spain, Landform Analysis, 17,
573 91-97, 2011.
574 Martínez, S., Ortiz, J., and Gil, M. L.: Geometric documentation of historical pavements
575 using automated digital photogrammetry and high-density reconstruction algorithms,
576 Journal of Archaelogical Science, 53, 1-11. 2015.
577 Martínez-Casasnovas, J. A. and Ramos, M. C.: Erosión por cárcavas y barrancos en el área de
578 viña del Alt Penedés-Anoia (NE España), Cuadernos de Investigación Geográfica, 35 (2),
579 223-238, 2009.
580 Martínez-Murillo, J. F., Nadal-Romero, E., Regüés, D., Cerdà, A., and Poesen, J.: Soil
581 erosion and hydrology of the western Mediterranean badlands throughout rainfall
582 simulation experiments: A review, Catena, 106, 101-112, 2013.
583 Marzolff, I., and Poesen, J.: The potential of 3D gully monitoring with GIS using high-
584 resolution aerial photography and a digital photogrammetry system, Geomorphology, 111,
585 48-60, 2009.
586 Mathys, N., Brochot, S., Meunier, M., and Richard, D.: Erosion quantification in the small
587 marly experimental catchments of Draix (Alpes de Haute Provence, France). Calibration
588 of the ETC rainfall-runoff-erosion model, Catena, 50 (2-4), 527-548, 2003.
589 Michetti, N., Chandler, J.H., and Lane, S.N.: Investigating the geomorphological potential of
590 freely available and accessible structure-from-motion photogrammetry using a
591 smartphone, Earth Surface Processes and Landforms, 40, 473-486, 2015.
592 Nadal-Romero, E., Martínez-Murillo, J.F., Vanmaercke, M., and Poesen, J.: Scale-
593 dependency of sediment yield from badland areas in Mediterranean environments, Prog.
594 Phys. Geogr., 35 (3), 297-332, 2011.

595 Nadal-Romero, E., Martínez-Murillo, J.F., Vanmaercke, M., and Poesen, J.: Corrigendum to
596 Scale-dependency of sediment yield from badland areas in Mediterranean
597 environments"(Progress in Physical Geography 35 (3) (2011), 297-332), Prog. Phys.
598 Geogr. 38 (3), 381-386, 2014.
599 Nadal-Romero, E. and Regüés, D.: Geomorphological dynamics of subhumid mountain
600 badland areas – weathering, hydrological and suspended sediment transport processes: a
601 case study in the Araguás catchment (Central Pyrenees) and implications for altered
602 hydroclimatic regimes, Prog. Phys. Geogr. 34 (2), 123-150, 2010.
603 Nadal-Romero, E., Latron, J., Martí-Bono, C., and Regüés, D.: Temporal distribution of
604 suspended sediment transport in a humid Mediterranean badland area: the Araguás
605 catchment, Central Pyrenees, Geomorphology, 97, 601-616, 2008.
606 Nadal-Romero, E., Regüés, D., Martí-Bono, C., and Serrano, P.: Badland dynamics in the
607 Central Pyrenees: temporal and spatial patterns of weathering processes. Earth Surface
608 Processes and Landforms 32, 888-904, 2007.
609 Nadel, D., Filim S., Rosenberg, D., Miller, V.: Prehistoric bedrock features: Recent advances
610 in 3D characterization and geometrical analyses, Journal of Archaeological Science, 53,
611 331-344, 2015.
612 Perroy, R.L., Bookhagen, B., Asner, G., Chadwick, O.A.: Comparison of gulyy erosion
613 estimates using airborne and ground-based LiDAR on Santa Cruz Island, California,
614 Geomorphology, 118, 288-300.
615 Prokop, A.: Assessing the applicability of terrestrial laser scanning for spatial snow depth
616 measurements, Cold Regions Science and Technology ,54, 155-163, 2008.
617 Pulice, I., Di Leob, P., Robustellia, G., Scarcigliaa, F., Cavalcanteb, F., and Belvisob, C.:
618 Control of climate and local topography on dynamic evolution of badland from southern
619 Italy (Calabria), Catena 109, 83-95, 2013.
620 Regüés, D., and Gallart, F.: Seasonal patterns of runoff and erosion responses to simulated
621 rainfall in a badland area in Mediterranean mountain conditions (Vallcebre, Southeastern
622 Pyrenees), Earth Surface Processes and Landforms, 29, 755–67, 2004.
623 Revuelto, J., López-Moreno, J. I., Azorin-Molina, C., Zabalza, J., Arguedas, G., and Vicente-
624 Serrano, S. M.: Mapping the annual evolution of snow depth in a small catchment in the
625 Pyrenees using the long-range terrestrial laser scanning, J. Maps 0, 1-15, 2014.
626 Sadiki, A., Faleh, A., Navas, A., and Bouhlassa, S.: Assessing soil erosion and control factors
627 by the radiometric technique in the Boussouab catchment, Eastern Rif, Morocco, Catena,
628 71 (1), 13-20, 2007.

629 Saez, J. L., Corona, C., Stoffe, M., Rovéra, G., Astrade, L., and Berger, F.: Mapping of
630 erosion rates in marly badlands based on a coupling of anatomical changes in exposed
631 roots with slope maps derived from LiDAR data, Earth Surf. Process. Landf., 36 (9),
632 1162-1171, 2011.
633 Sirvent, J., Desir, G., Gutierrez, M., Sancho, C., and Benito, G.: Erosion rates in badland
634 areas recorded by collectors, erosion pins and profilometer techniques (Ebro Basin, NE-
635 Spain), Geomorphology, 18 (2), 61-75, 1997.
636 Smith, M.W., and Vericat, D.: From experimental plots to experimental landscapes:
637 topography, erosion and deposition in sub-humid badlands from Structure-from-Motion
638 photogrammetry, Earth Surf. Process. Landforms DOI: 10.1002/esp.3747, 2015.
639 Vergari, F., Della Seta, M., Del Monte, M., Fredi, P., and Lupia Palmieri, E.: Long- and
640 short-term evolution of several Mediterranean denudation hot spots: The role of rainfall
641 variations and human impact, Geomorphology, 183, 14-27, 2013.
642 Verhoeven, G., Taelman, D., Vermeulen, F.: Computer Vision-based orthophoto mapping of
643 complex archaological sites: The ancient quarry of Pitaranha, Archaeometry, 54, 1114-
644 1129, 2012.
645 Vericat, D., Smith, M. W., and Brasington, J.: Patterns of topographic change in sub-humid
646 badlands determined by high resolution multi-temporal topographic surveys, Catena, 120,
647 164-176, 2014.
648 Walling, D. E.: Drainage basin studies, in: Field experiments and measurement programs in
649 geomorphology, Slaymaker, O. (Eds.), Balkema, Rotterdam, 17-60, 1991.
650 Westoby, M.J., Brasington, J., Glasser, N.F., Hambrey, M.J., and Reynolds, J.M.: "Structure-
651 from-Motion" photogrammetry: A low-cost, effective tool for geoscience application,
652 Geomorphology, 179, 300-314, 2012.
653 Yamakoshi, T., Mathys, N., and Klotz, S.: Time-lapse video observation of erosion processes
654 on the Black Marls badlands in Southern Alps, France, Earth Surface Processes and
655 Landforms, 34, 314–18, 2009.
656

	Monitoring interval	Number of days	Total rainfall (mm)	Max. daily rainfall (mm)	Max. rainfall 5-min intensity (mm h^{-1})
Period 1	23 July 2013-12 Nov. 2013	112	334.8	77.2	148.8
Period 2	12 Nov. 2013- 26 Mar. 2014	134	308.8	24.6	14.4
Period 3	26 Mar. 2014- 23 July 2014	119	198	30.2	33.6
Annual period	23 July 2013-23 July 2014	365	841.6	77.2	148.8

Table 1. Summary of time intervals and rainfall data recorded during the monitoring periods

North-facing slope		Period 1	Period 2	Period 3	July 2013-July 2014
TLS	Mean ± SD (m)	-0.020 ± 0.032	-0.046 ± 0.050	-0.012 ± 0.027	**-0.077 ± 0.049**
	Max + (m)	0.31	0.25	0.14	**0.25**
	Max - (m)	-0.61	-0.39	-0.28	**-0.59**
Photogrammetry	Mean ± SD (m)	-0.035±0.044	-0.051 ± 0.042	-0.003 ± 0.025	**-0.017 ± 0.038**
	Max + (m)	0.41	0.16	0.21	**0.34**
	Max - (m)	-0.43	-0.39	-0.25	**-0.46**

Table 2. Mean differences, standard deviation and maximum differences (Max+, deposition; Max-, erosion) of point clouds obtained for different survey periods with TLS and photogrammetry on north-facing slopes

South-facing slope		Period 1	Period 2	Period 3	July 2013-July 2014
TLS	Mean ± SD (m)	-0.006±0.026	-0.037±0.066	0.011±0.027	**-0.032±0.071**
	Max + (m)	0.179	0.52	0.24	**0.42**
	Max - (m)	-0.194	0.416	-0.176	**-0.45**
Photogrammetry	Mean ± SD (m)	-0.010±0.025	0.001±0.055	0.011±0.0211	**-0.002±0.056**
	Max + (m)	0.18	0.48	0.22	**0.48**
	Max - (m)	-0.22	-0.42	-0.17	**-0.42**

Table 3. Mean differences, standard deviation and maximum differences (Max+, deposition; Max-, erosion) of point clouds obtained for different survey periods with TLS and photogrammetry on south-facing slopes

	24/07/2013	24/07/2014
North-facing slopes (TLS-SfM) [m]	**-0.013 ± 0.0308**	**-0.0201± 0.0326**
South- facing slope (TLS-SfM) [m]	**-0.002 ± 0.0202**	**-0.006 ± 0.0141**

741

742 **Table 4. Mean differences and standard deviation of point clouds obtained with both methods calculated**
743 **for the first and last acquisition dates (23/07/13 and 23/07/14).**

744

745

746

747

748

749

750

751

752

753

754

755

756

757

758

759

760

761

762

763

764

765

766

	Advantage	Disadvantage
TLS	• non-invasive • pinpoint accuracy • high accuracy potential and automation level • high data adquisition • post-processing is fast	• high economic cost • heavy material (difficulties for portability) • longer measure time • problems with little misalignments of reference points • sight shadowing
Photogrammetry	• non-invasive • low costs • small format: low weight • reduce data collection time by ~80% • high number of photos to minimize missing areas	• centimetric accuracy • worse adaptation to survey large areas • post-processing is still labor-intensive • problems with illumination changes

Table 5. Advantages and disadvantages of Terrestrial Laser Scanner (TLS) and Photogrammetry methodologies for studying geomorphological processes in badland areas.

Figure 1. Distribution of soil erosion studies in badland areas according to different methodologies

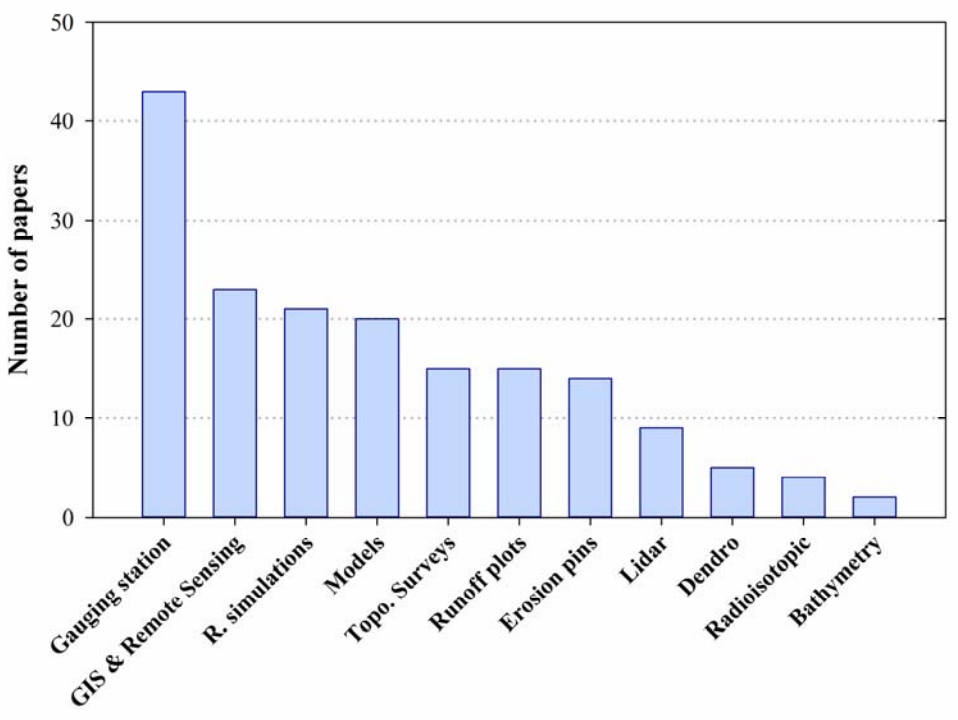

Figure 2. Evolution of different methodologies and difference between invasive and non-invasive methods

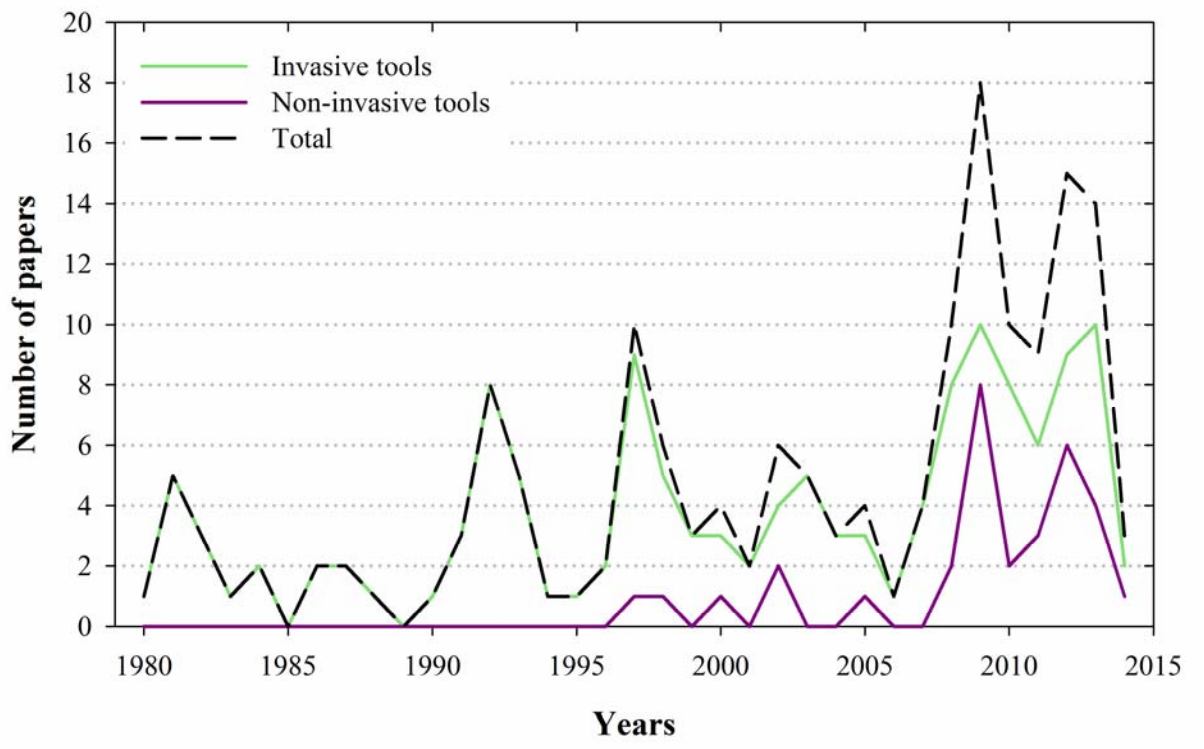

834 Figure 3. Field site location, Araguás catchment. Detailed image of both selected slopes

835

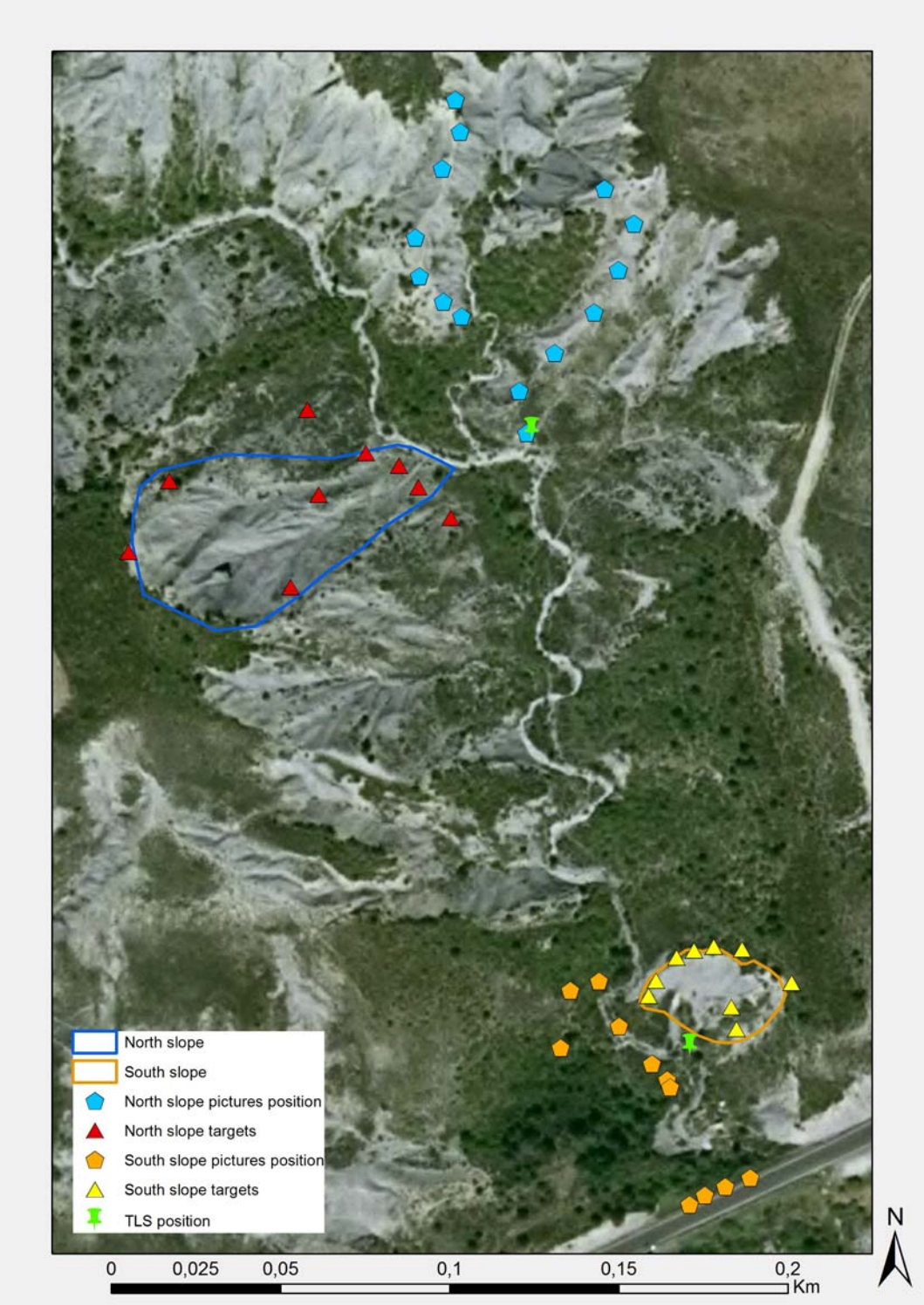

836

837

838

839

Figure 4. Daily rainfall and accumulated rainfall during the survey period (July 2013–July 2014).

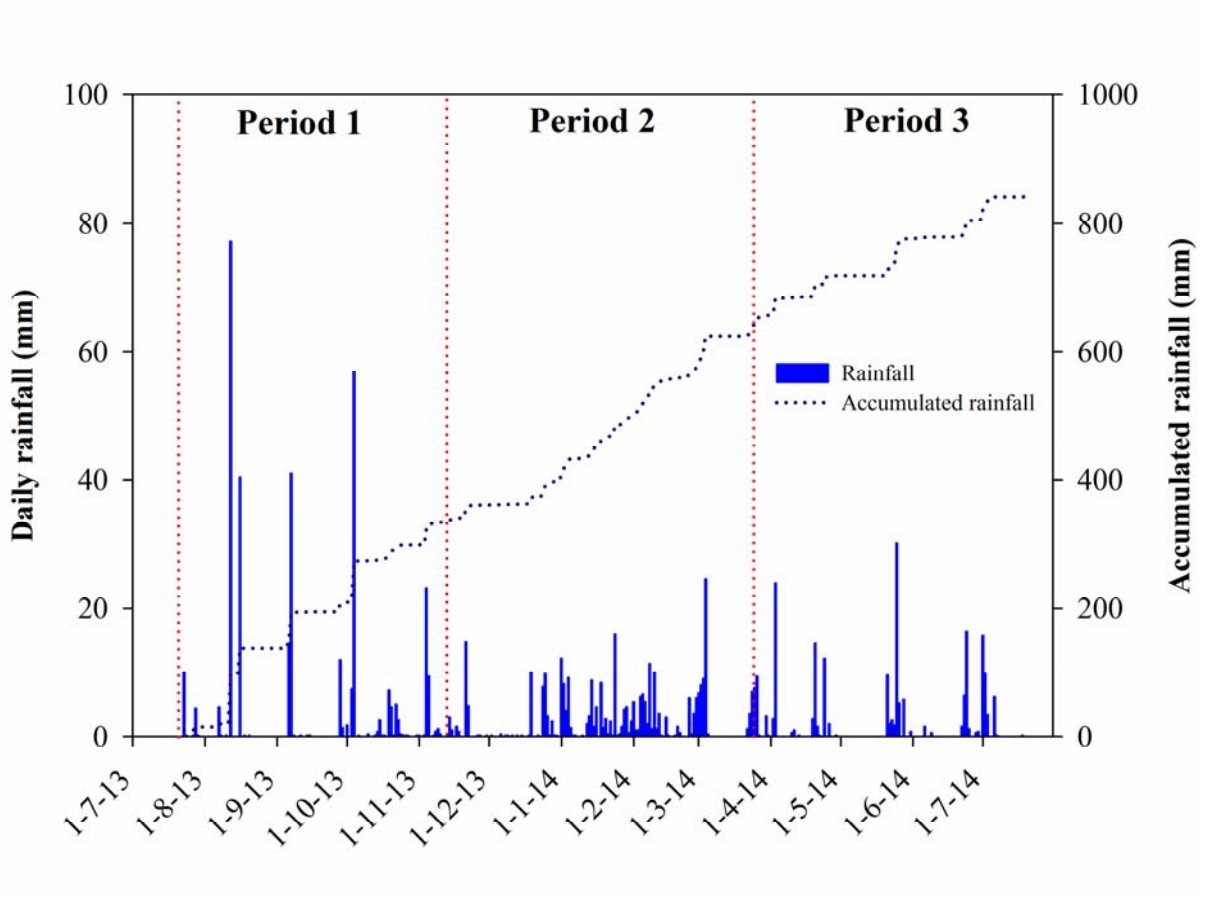

Figure 5. Topographic changes observed at the monitoring intervals and at annual scale obtained with TLS on north-facing slopes (CloudCompare software).

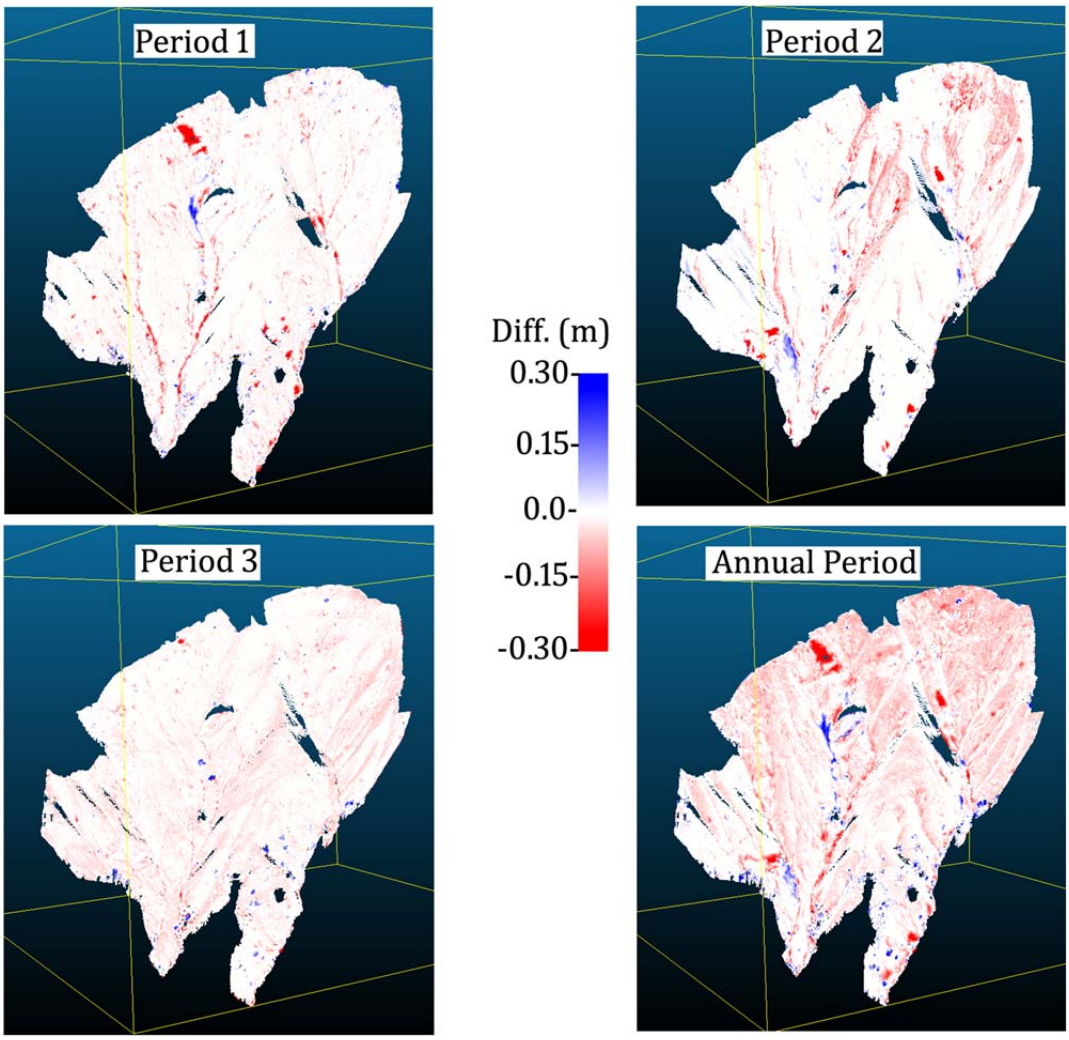

Figure 6. Topographic changes observed at the monitoring intervals and at annual scale obtained with photogrammetry on north-facing slopes (CloudCompare software).

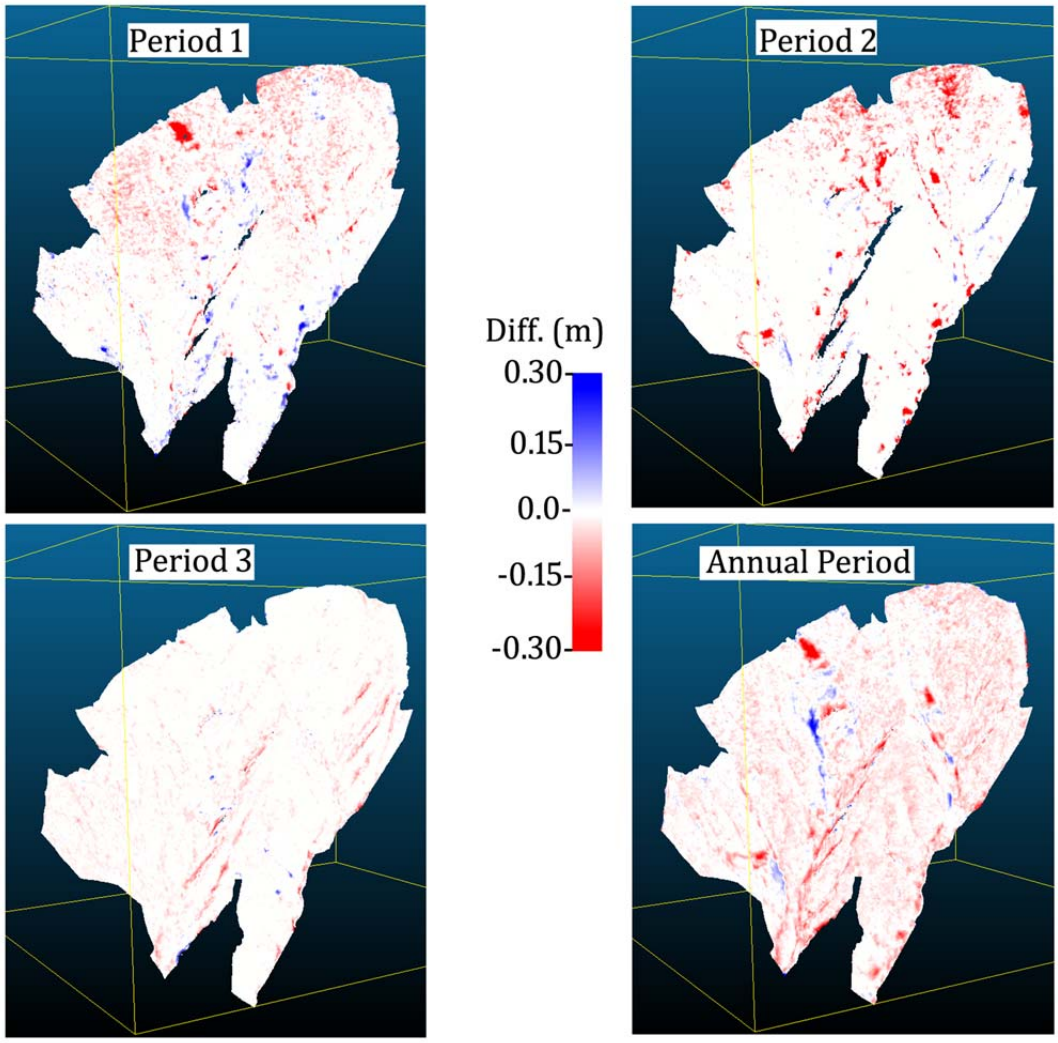

Figure 7. Topographic changes observed at the monitoring intervals and at annual scale obtained with TLS on south-facing slopes (CloudCompare software).

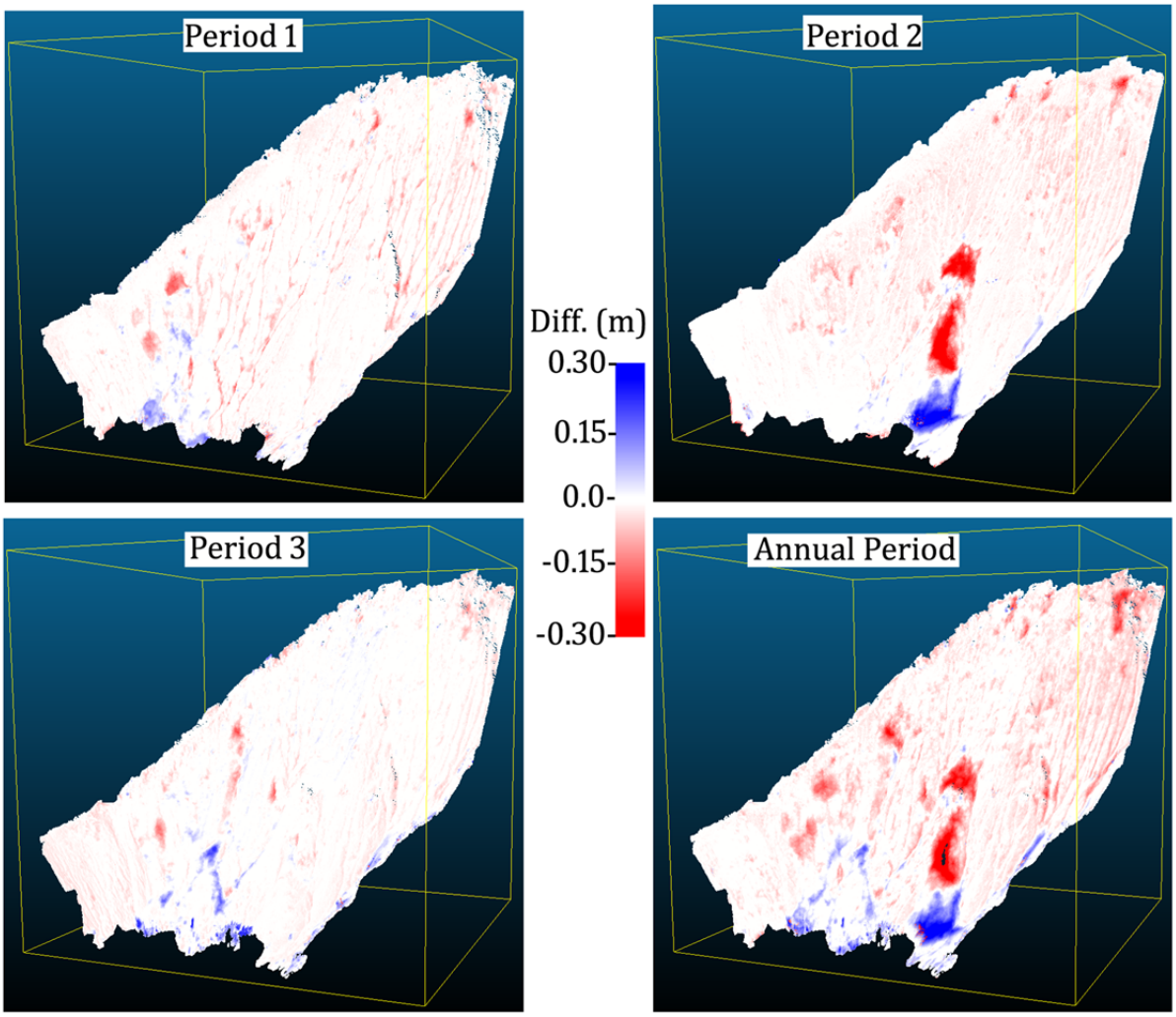

Figure 8. Topographic changes observed at the monitoring intervals and at annual scale obtained with SfM on south-facing slopes (CloudCompare software).

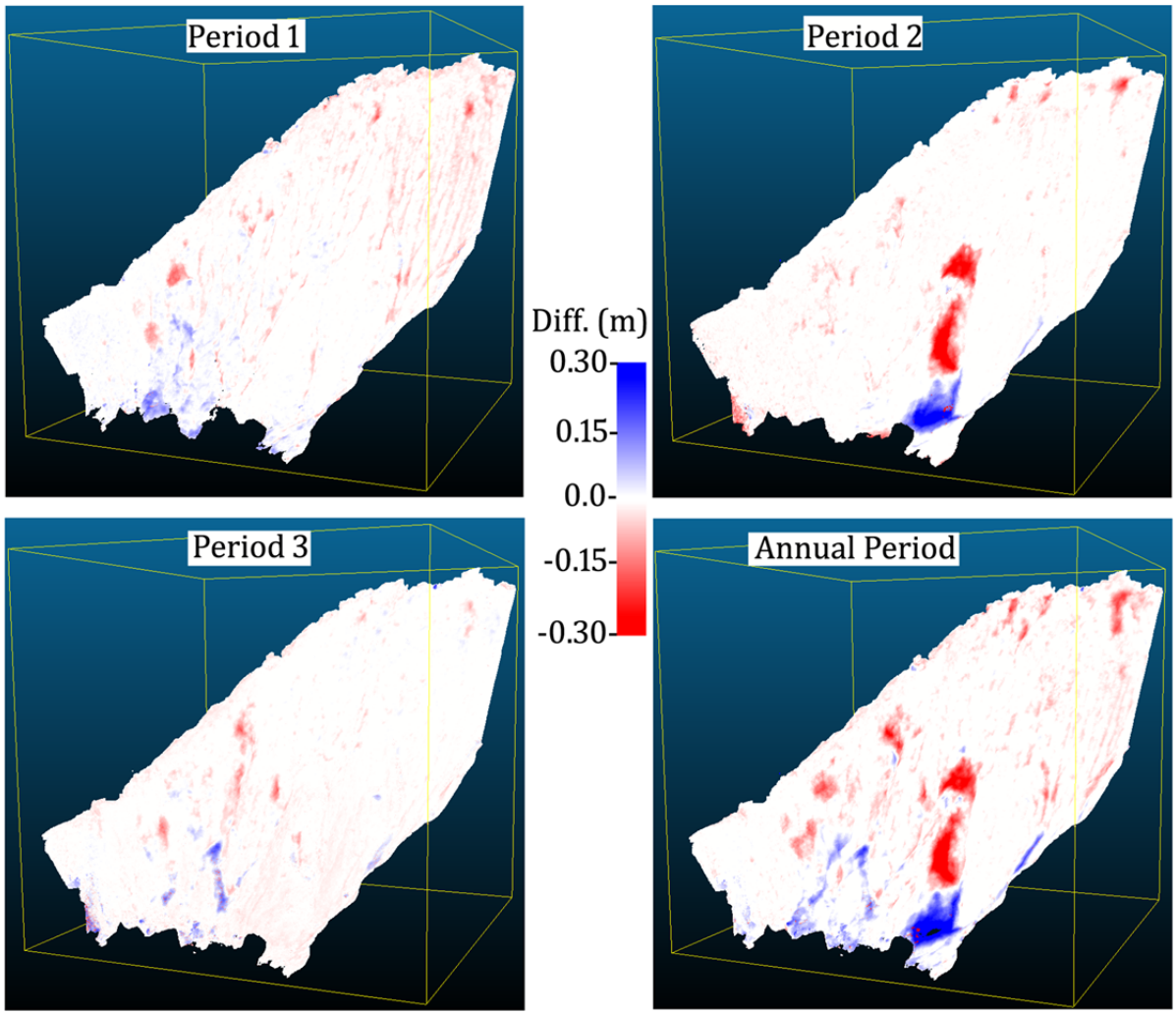

Figure 9. Comparison of DEMs between techniques, considering TLS as the reference, on north-facing slopes. Differences have been calculated for the first and last acquisition dates (23/07/13 and 23/07/14) (cloud compare software). A RGB colored points images is added in right panel as an overview of the north-facing slopes

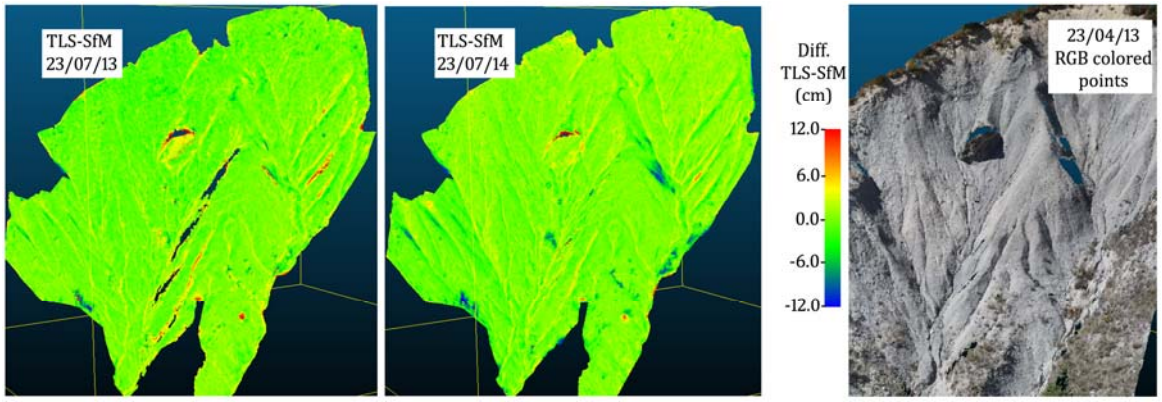

Figure 10. Comparison of DEMs between techniques, considering TLS as the reference, on south-facing slopes. Differences have been calculated for the first and last acquisition dates (23/07/13 and 23/07/14) (cloud compare software). A RGB colored points images is added in right panel as an overview of the south-facing slopes